

ON THE DESIGN OF SHOCK-FREE, TRANSONIC, SLENDER BODIES OF REVOLUTION

by Ron Buckmire *

*Mathematics Department
Occidental College
Los Angeles, CA 90041, U.S.A.*

In this paper a procedure to design shock-free, transonic, slender bodies of revolution will be detailed. Using transonic small-disturbance theory, a boundary-value problem is developed describing flow around the body in the physical plane and then transformed into the hodograph plane. In the hodograph plane, spatial variables depend on velocity components, instead of the usual dependence of velocity components upon spatial variables in the physical plane. The transformed boundary-value problem is solved numerically using finite-difference approximations and iterative methods. Several shock-free bodies are computed, with differing values of the transonic similarity parameter, $K = (1 - M_\infty^2)/\delta^2 M_\infty^2$, where M_∞ is the flow Mach number and δ is the body thickness.

There are advantages to designing shock-free bodies in the hodograph plane. There is a very simple criterion for detecting when a shock-free flow has been computed in the hodograph: the jacobian of the mapping from physical plane to hodograph plane must be negative everywhere. A difficult Neumann-type boundary condition at the origin of the physical plane becomes a simpler Dirichlet boundary condition in the hodograph. In the physical plane, the body shape is represented by a source distribution of singularities along the origin and the exact locations of the subsonic and

supersonic regions of the flow are unknown a priori. This makes perturbing the shape to construct a shock-free body difficult. In the hodograph body shape the solution is less sensitive to changes along the sonic line and the location of this boundary is known precisely, which makes design in the hodograph plane more desirable.

The importance of computing shock-free bodies of revolution follows from the Transonic Area Rule, which implies that flows around bodies with equivalent rates of change of cross-sectional area possess equivalent flows. Thus computation of shock-free bodies of revolution may be used to design other bodies which are shock-free or have dramatically reduced drag.

Introduction

This paper describes a procedure to construct or design slender bodies of revolution which possess shock-free flows in the transonic domain. The basic idea is to construct a body over which a flow at near-sonic speeds is accelerated at the nose and decelerated before it reaches the tail without an intervening shock. There has been a fair amount of previous work on shock-free transonic flows, from the first experimental results of Pearcey^[16] and Whitcomb and Clark,^[19] to the shock-free quasi-elliptical wing section of Nieuwland^[15] and, of course, the theoretical results of Bauer *et al.*^[1, 2, 3] which were confirmed by the wind tunnel experiments of Kacprzynski

*The author can be reached by electronic mail at ron@abacus.oxy.edu. Copyright ©1998 by Ron Buckmire. Published by the American Institute of Aeronautics and Astronautics, Inc., with permission.

et al.^[11, 12, 13] However, all these investigations involved two-dimensional flows. In 1990, Cole & Schwendeman^[10] announced the first computation of a shock-free transonic flow in more than two dimensions with the construction of their fore-aft-symmetric slender body of revolution. In 1994, Buckmire^[4] extended this work with the computation of several fore-aft asymmetric shock-free bodies. This paper will systematically detail an algorithm which can be used to compute slender bodies of revolution which possess shock-free flows.

The procedure outlined will result in a body shape function $F(x)$, or an equivalent source distribution function $S(x)$, which is shock-free at a given value of the transonic similarity parameter K (which depends on δ and M_∞).

Mathematical formulation

In the process of designing slender bodies of revolution which possess shock-free flows an assumption of steady, inviscid, compressible, potential flow is made and the problem is formulated using transonic small-disturbance theory as found in the work of Cole and Cook^[6].

The exact velocity potential is expressed as an asymptotic expansion in δ (the body thickness) and M_∞ (the flow Mach number) involving the disturbance potential $\phi(x, \bar{r})$, where $\bar{r} = \delta M_\infty r$. Using a triple-deck asymptotic analysis, a boundary-value problem for $\phi(x, \bar{r})$ consisting of an elliptic-hyperbolic partial differential equation (the Kármán-Guderley equation (1) in cylindrical coordinates), a singular inner Neumann boundary condition (2) at $r = 0$ and a non-singular outer Dirichlet boundary condition (3) far away from $r = 0$ is formulated. The mathematical description of the boundary-value problem is given below.

$$(K - (\gamma + 1)\phi_x)\phi_{xx} + \phi_{\bar{r}\bar{r}} + \frac{1}{\bar{r}}\phi_{\bar{r}} = 0. \quad (1)$$

As $\bar{r} \rightarrow 0$ and $|x| \leq 1$,

$$\phi(x, \bar{r}) \rightarrow S(x) \log \bar{r} + G(x) + \dots \quad (2)$$

As $(x^2 + \bar{r}^2)^{1/2} \rightarrow \infty$,

$$\phi(x, \bar{r}) \rightarrow \frac{D}{4\pi} \frac{x}{(x^2 + K\bar{r}^2)^{3/2}} \quad (3)$$

In (1), (2) and (3) the variable \bar{r} is a scaled cylindrical coordinate, K is the transonic similarity parameter, D is a dipole strength and $\phi(x, \bar{r})$ is a velocity disturbance potential. These equations describe a three-dimensional flow but by using cylindrical coordinates and an axisymmetric body only two independent variables are needed.

Complete details of the derivation of the boundary-value problem in the physical plane are given by Buckmire^[4] but there are some points which are important enough to describe here.

Note that the outer boundary condition (3) is derived using asymptotic matching and far away from the body velocity perturbations attenuate ($\phi_x^2 + \phi_{\bar{r}}^2 \rightarrow 0$) so that to a first approximation the far-field flow can be thought of as Prandtl-Glauert flow around a closed body, which is represented by a dipole. The strength D of this dipole is the sum of two parts, D_{body} and D_{flow} , given by

$$D_{body} = \pi \int_{-1}^{+1} F^2(x) dx \quad (4)$$

and

$$D_{flow} = \pi(\gamma + 1) \int_{-\infty}^{\infty} \int_0^{\infty} \phi_x^2(x, \bar{r}) \bar{r} dx d\bar{r}. \quad (5)$$

Also note that the inner boundary condition (2) results from an asymptotic matching of the inner expansion and yields an important expression for the source distribution,

$$S(x) = F(x)F'(x) = \frac{1}{2\pi} \frac{dA^*}{dx}, \quad (6)$$

where $A^* = \pi F^2(x)$ is the scaled cross-sectional area of the body. Thus the source distribution can be computed directly from the given body shape and it represents the rate of change of cross-sectional area of the body. The function $G(x)$ which occurs in (2) needs to be computed very accurately, because the pressure coefficient on the body $C_{p_{body}}$ depends directly on $G'(x)$,

$$C_{p_{body}}(x) = -\delta^2 \{2S'(x) \log(\delta^2 M_\infty F(x)) + 2G'(x) + (F'(x))^2\}. \quad (7)$$

Dealing with the inner boundary condition (2) is complicated by the fact that $\phi(x, \bar{r})$ and $S(x) \log \bar{r}$

are becoming singular as $\bar{r} \rightarrow 0$, which is where this boundary condition must be evaluated. A special numerical scheme discussed in [5] was developed to accurately compute this singular boundary condition as $\bar{r} \rightarrow 0$. However, even this new numerical scheme can not overcome the fact that solutions of the boundary-value problem for ϕ are extremely sensitive to perturbations in the body shape (which affects $S(x)$). This sensitivity makes direct design in the physical plane difficult, so, the boundary-value problem for $\phi(x, \bar{r})$ is transformed to the hodograph plane. Complete details of this transformation are given in [10] compared to the brief description here.

Choosing the variables

$$w = (\gamma + 1)\phi_x - K, \quad \vartheta = (\gamma + 1)\phi_{\bar{r}}$$

$$R = \frac{\bar{r}^2}{2}, \quad \nu = \bar{r}\vartheta \quad (8)$$

the transonic small-disturbance equation (1), abbreviated TSDE, can be re-written as a first-order system

$$\begin{cases} ww_x = \nu R \\ 2Rw_R = \nu_x \end{cases} \quad (9)$$

and (9) can be transformed to the hodograph plane by reversing the relationship between the spatial coordinates (x, \bar{r}) and the velocity components (w, ν) to produce

$$\begin{cases} wR_\nu = x_w \\ 2Rx_\nu = R_w \end{cases} \quad (10)$$

The Jacobian of the hodograph transformation is given by

$$J = \frac{\partial(x, R)}{\partial(w, \nu)} = x_w R_\nu - x_\nu R_w \quad (11)$$

which, using information from (10) can be written as

$$J(w, \nu) = wR_\nu^2 - \frac{R_w^2}{2R} \quad (12)$$

Notice that since R is non-negative by definition in (8) $J < 0$ when $w < 0$ and that this corresponds to subsonic flow, i.e. $\phi_x < K/(\gamma + 1)$. For the transformation from the physical plane to the hodograph plane to be smooth it is required that the Jacobian J must be negative when $w \geq 0$ also.

The intransigence of the sign of the Jacobian will be the basic condition which determines whether a shock-free solution has been computed.

The new system (10) can be re-written as the hodograph version of the TSDE by eliminating x to yield

$$\left(\frac{R_w}{2R}\right)_w - wR_{\nu\nu} = 0. \quad (13)$$

The hodograph TSDE (13) is solved for $R(w, \nu)$ like the physical TSDE (1) was to be solved for $\phi(x, \bar{r})$. The governing PDE is quasi-linear in both planes but the boundary conditions in the hodograph plane are easier to deal with.

The Hodograph Plane

To gain a better understanding of the hodograph topology and the differences between the physical boundary-value problem for $\phi(x, \bar{r})$ and the hodograph boundary-value problem for $R(w, \nu)$ examine Figure 1.

The physical plane consisting of an infinite half-plane $0 < \bar{r} < \infty, |x| < \infty$ is transformed to an infinite strip $|w| < \infty, \nu^* < \nu < \nu_*$ in the hodograph plane. Notice how the points labelled I (i.e. infinity) get mapped to a single point. Notice also how the body with nose N and tail T gets mapped. Contours of \bar{r} in the physical plane are represented by a thick dashed line and a dotted line, both of which are then shown in the hodograph as corresponding contours of R . Once the topology of the transformation is understood attention must be focussed on comprehending how the physical boundary-value problem changes when it is transformed into the hodograph.

Near-field boundary condition

The inner boundary condition on $\phi(x, \bar{r})$ in the physical plane as $\bar{r} \rightarrow 0$ becomes the condition on $R \rightarrow 0$ as $w \rightarrow \pm\infty$ in the hodograph. Therefore the asymptotic behavior of ϕ as $\bar{r} \rightarrow 0$ needs to be closely examined in order to obtain the asymptotic behavior of $R(w, \nu)$ as $w \rightarrow \pm\infty$. This behavior of the flow close to the body with $\bar{r} \rightarrow 0$ is often referred to as the "near-field behavior."

Recall that the asymptotic behavior of the disturbance potential near the body (as $\bar{r} \rightarrow 0$) was

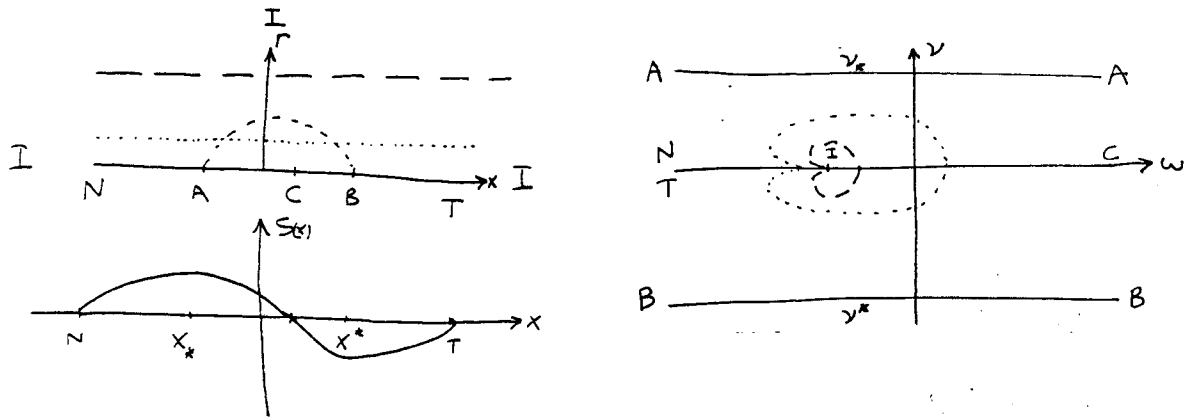


Figure 1: Mapping the boundary-value problem to the hodograph plane

given by

$$\phi(x, \bar{r}) = S(x) \log \bar{r} + G(x), \quad \bar{r} \rightarrow 0, \quad |x| < 1$$

which can be differentiated to yield

$$\left\{ \begin{array}{l} \nu = (\gamma + 1) \bar{r} \frac{\partial \phi}{\partial \bar{r}} \\ \quad = (\gamma + 1) S(x) + \dots \\ w + K = (\gamma + 1) \frac{\partial \phi}{\partial x} \\ \quad = (\gamma + 1) S'(x) \log \sqrt{2R} + \\ \quad \quad (\gamma + 1) G'(x) + \dots \end{array} \right\} \quad (14)$$

which makes it clear that as $R \rightarrow 0, \nu \rightarrow (\gamma + 1) S(x)$ and $w \rightarrow +\infty$ when $S'(x) < 0$ but $w \rightarrow -\infty$ when $S'(x) > 0$. A typical source distribution function $S(x)$ is given in Figure 2, and it possesses two extrema, $x^* < 0$ and $x_* > 0$ where $S' = 0$. These values determine the width of the hodograph strip, which is $\nu^* \leq \nu \leq \nu_*$ where $\nu^* = (\gamma + 1) S(x^*)$ and $\nu_* = (\gamma + 1) S(x_*)$.

The functional form of the near-field behavior of $R(w, \nu)$ approaching zero as $w \rightarrow \pm\infty$ can be obtained by inverting the relationship given in (14) and keeping the dominant terms. This gives

$$\left\{ \begin{array}{l} R(w, \nu) = A(\nu) e^{B(\nu)w} + \dots \\ x(w, \nu) = C(\nu) + \dots \end{array} \right\}, \quad (15)$$

where

$$A(\nu) = \frac{1}{2} \exp [B(\nu) (K - (\gamma + 1) G'(C(\nu)))]$$

$$B(\nu) = \frac{2}{(\gamma + 1) S'(C(\nu))}$$

$$C(\nu) = \text{inverse function of } (\gamma + 1) S(x).$$

The form of the function $C(\nu)$ changes depending on which side of the hodograph strip it is evaluated on. This is obvious by looking at Figure 2 and recalling that $C(\nu)$ is essentially the inverse of the function plotted. It can be defined as

$$C(\nu) = \begin{cases} C_{left}(\nu) & \text{if } w \rightarrow -\infty \text{ and } \nu^* \leq \nu \leq \nu_* \\ C_{right}(\nu) & \text{if } w \rightarrow +\infty \text{ and } \nu^* \leq \nu \leq \nu_* \end{cases}$$

where $C_{left}(\nu)$ and $C_{right}(\nu)$ are plotted in Figure 2. In order to invert the source distribution function $S(x)$ it is necessary to first realize that it consists of two parts, the segment labelled AB and the union of segments labelled NA and BT form the second part. The part consisting of NA and BT gets mapped to $w = -\infty$ in the hodograph plane and represents the part of the body on which the flow is subsonic, while the segment AB gets mapped to $w = +\infty$ and represents the part of the body on which the flow is supersonic.

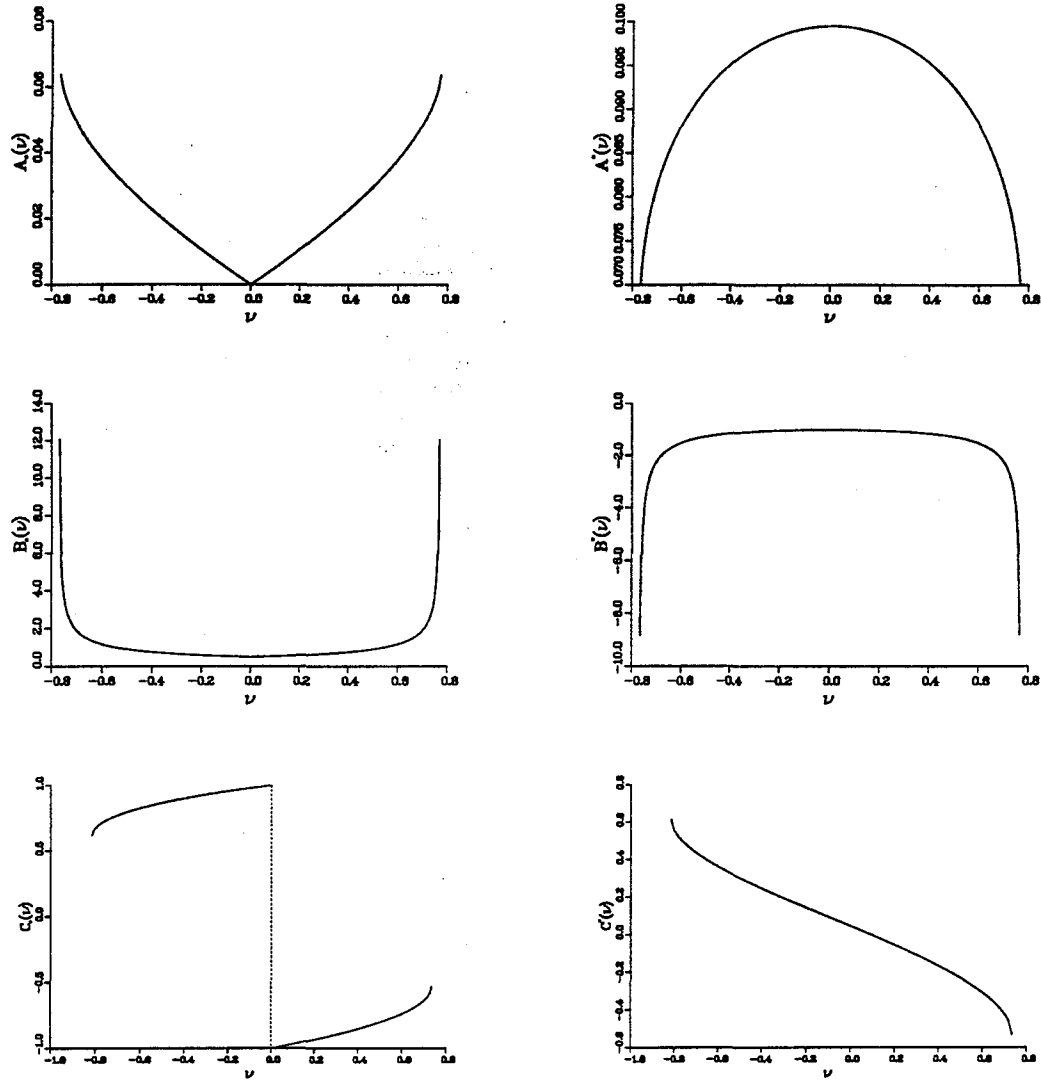


Figure 2: Graphs of $A(\nu)$, $B(\nu)$ and $C(\nu)$ showing different branches at $\pm\infty$

Far-field boundary condition

From observing (3) it can be shown that the far-field in the physical plane (the area far away from the body, where $x^2 + \bar{r}^2 \rightarrow \infty$ and $\phi_x, \phi_{\bar{r}} \rightarrow 0$) gets mapped to the single coordinate $w = -K, \nu = 0$ in the hodograph plane. This point is often called the *free-stream singularity*. As stated previously, the far-field flow is assumed to resemble dipole flow, since far away from the body the governing PDE becomes the Prandtl-Glauert equation around a closed body. Substituting the expression for ϕ from (3) in (8), the far-field boundary condition in the hodograph becomes represented implicitly by the system

$$\left\{ \begin{array}{l} \nu = (\gamma + 1)\bar{r} \frac{\partial \phi}{\partial \bar{r}} \\ = -(\gamma + 1) \frac{\mathcal{D}}{4\pi} \frac{6KR}{(x^2 + 2KR)^{5/2}} \\ w + K = (\gamma + 1) \frac{\partial \phi}{\partial x} \\ = (\gamma + 1) \frac{\mathcal{D}}{4\pi} \frac{2KR - 2x^2}{(x^2 + 2KR)^{5/2}} \end{array} \right. \quad (16)$$

which, for given values of (w, ν) near the free-stream singularity, can be solved numerically for $R(w, \nu)$. In addition, \mathcal{D}_{flow} can be expressed in hodograph variables as

$$\mathcal{D}_{flow} = \frac{\pi}{\gamma + 1} \int_{-\infty}^{\infty} \int_{\nu_*}^{\nu^*} |J|(w + K)^2 dw d\nu \quad (17)$$

In Figure 1 the qualitative behavior of $R(w, \nu)$ near the free stream singularity at $(-K, 0)$ is indicated by depicting a dotted line on which R is constant in both the physical plane and the hodograph plane.

The Numerical Method

A numerical method to solve the hodograph TSDE (13) and its associated boundary conditions will be given in this section. The numerical method devised by Cole & Schwendeman^[10] is modified so that it can be applied to bodies without fore-aft symmetry. The basic idea recalls

the scheme used by Sobieczky et al.^[18]. In their scheme, the physical plane characteristic curves in the supersonic zone are computed from the sonic line down to the body and then flow parameters are altered to disentangle the characteristics in order to produce a shock-free solution. In the physical plane, the criterion for a shock-free flow is the appearance of no discontinuities in the flow. Clearly, if the characteristic curves intersect then this represents a discontinuity and is indicative of a shocked flow. In the hodograph plane, the criterion for a shock-free flow is that the Jacobian of the transformation is strictly negative at all points in the plane. The numerical method in this paper, like Sobieczky's method, also involves choosing values along the sonic line and computing the solution in the hyperbolic (supersonic) region of the flow. However, the advantages of executing the design of the shock-free flow in the hodograph plane is that the location of the sonic line is known *a priori*, and the condition for shocklessness is simpler. It is well-known that in the physical plane numerical calculations are quite sensitive to perturbations of the flow parameters. Also, in the physical plane finding the location of the boundary between subsonic and supersonic zones, the sonic line, is an implicit problem since it requires knowing the disturbance potential which is what you are solving for at the time.

To begin the design procedure a number of parameters must be inputted, such as the free-stream Mach number, the dipole strength and the body shape. This corresponds to setting the value of K , \mathcal{D} and $F(x)$. From $F(x)$ one can immediately obtain $S(x)$ and, more importantly, the coordinates of its extrema, x^* and x_* . These values are used to compute ν^* and ν_* , which determine the width of the hodograph strip.

The hodograph TSDE (13) is discretized using a standard second-order finite-difference scheme and the implicit Dirichlet condition near the free-stream singularity at $(-K, 0)$ and the Dirichlet condition of $R(w, \nu^*) = 0$ and $R(w, \nu_*) = 0$ are implemented. By choosing $S(x)$ in the physical plane, the corresponding function $C(\nu)$ and $B(\nu)$ has been defined as detailed in (15). Using the branch of $B(\nu)$ which uses $C_{left}(\nu)$ the boundary

condition for $R(w, \nu)$ as $w \rightarrow -\infty$ is approximated by using the condition

$$\frac{R_w}{R} = B_{left}(\nu) \text{ for } w \rightarrow -\infty \quad (18)$$

In practice, a discrete version of this condition (18) is evaluated at a moderate negative value of w because R approaches zero so quickly as $|w|$ becomes large.

The last boundary to be implemented in order to have a complete boundary value problem for R in the elliptical region of the hodograph (i.e. $w < 0$) is along the sonic line $w = 0$. Note that in the hodograph plane, it is known exactly where the sonic bubble lies, while in the physical plane one needs to implement Murman-Cole switching^[9] to compute the location of the sonic bubble. It is in this choice for the sonic line data, i.e. the value of the solution $R(0, \nu)$ where design choices are made. One choice for the form of $R(0, \nu)$ is a function $Q(z(\nu))$ which can be represented as

$$Q(z) = P(z) \exp \left[\frac{\sigma z^2}{1 - z^2} \right], \quad |z| \leq 1 \quad (19)$$

where

$$z(\nu) = \frac{2\nu - \nu_* - \nu^*}{\nu_* - \nu^*}, \text{ and}$$

$$P(z) = a_0 + a_1 z + a_2 z^2 + \dots, \text{ and } \sigma < 0.$$

The original functional form of $P(z; \{a_i\})$ is influenced by the function $A_{right}(\nu)$ but in practice the parameters $\{a_i\}$ will need to be adjusted to produce the final version of $Q(z)$. The elliptical boundary value problem for R is solved numerically using a combination of successive relaxation and Newton's method with the solution to the incompressible version of the equations serving as an initial condition. To obtain the numerical solution of the problem in the supersonic ($w > 0$) domain involves implementing a simple, explicit marching scheme, starting from the sonic line at $w = 0$ and integrating the now-hyperbolic hodograph TSDE (13) using the subsonic ($w < 0$) solution as an initial condition. At every step of the integration in the hyperbolic ($w > 0$) region a discrete version of the Jacobian is computed along with the solution and its sign is verified to be negative. If the

Jacobian ever becomes positive, the integration is halted. A non-negative Jacobian means a shock-free solution has not been found. The procedure is then repeated: new sonic line data for $R(0, \nu)$ is chosen by altering $Q(z)$, the subsonic boundary-value problem is solved, and integration into the hyperbolic region using the new solution is executed. If the Jacobian remains negative until w reaches a sufficiently large value (typically, as far out to positively as the boundary condition (18) was applied at " $w = -\infty$ ") then a shock-free numerical solution is said to have been computed.

After $R(w, \nu)$ has been computed numerically in the entire discretized hodograph strip a number of final calculations have to be made. The value of the dipole strength of the flow must be computed, and if necessary a fixed point iteration on \mathcal{D} is implemented, so that the computed dipole strength is same as the input dipole strength. After this, one uses R to find physical plane variables. In particular, this is accomplished by integrating the system of first-order equations given in (10). Of particular interest are S' , G' and F' which are used to compute $C_{P_{body}}(x)$ and $F(x)$, the body shape.

Algorithm

A step-by-step algorithm as first implemented by Buckmire^[4] is presented below which is equivalent to the description given above.

- 1 Choose body function $F(x)$
- 2 Calculate $S(x)$ and $S'(x)$
- 3 Find roots of $S'(x)$: x^* and x_* and use them to compute ν^* and ν_*
- 4 Discretize the hodograph strip as shown in Figure 1
- 5 Set near-field boundary conditions at $w = \pm\infty$
- 6 Choose the $P(z; \{a_i\})$ function to replace boundary condition at $w = +\infty$ with given sonic line data at $w = 0$
- 7 Assume a value for \mathcal{D} , the dipole strength: \mathcal{D}_{new}
- 8 Set far-field boundary conditions near the free stream singularity by solving the given implicit equations (3)

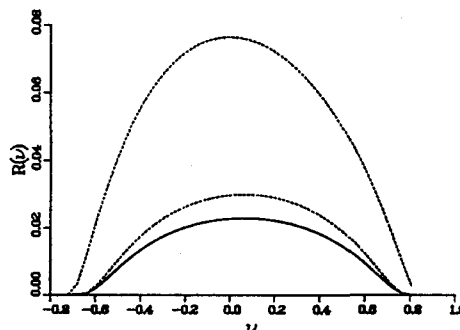


Figure 3: Sonic line data used to compute the SFB-1 solution

- 9 Choose an initial condition for R everywhere in the elliptic region
- 10 Solve the boundary value problem numerically for R in the elliptic region
- 11 Use time-like marching scheme to extend solution into hyperbolic region and check Jacobian is negative everywhere it is computed
- 12 If the computed Jacobian is greater than zero at any point, go to item 6 and iterate
- 13 Integrate to obtain a value for \mathcal{D}_{num} from the numerically generated flow field
- 14 If $|\mathcal{D}_{num} - \mathcal{D}_{new}|$ greater than tolerance, go to item 7 and iterate
- 15 Convert variables back into the physical plane: compute $F(x)$ and $S(x)$ from numerical solution. Also G' , S' , F' are all needed to compute $C_{p_{body}}$ and plot graphs of $F(x)$, $S(x)$ and $C_{p_{body}}$

Numerical Results

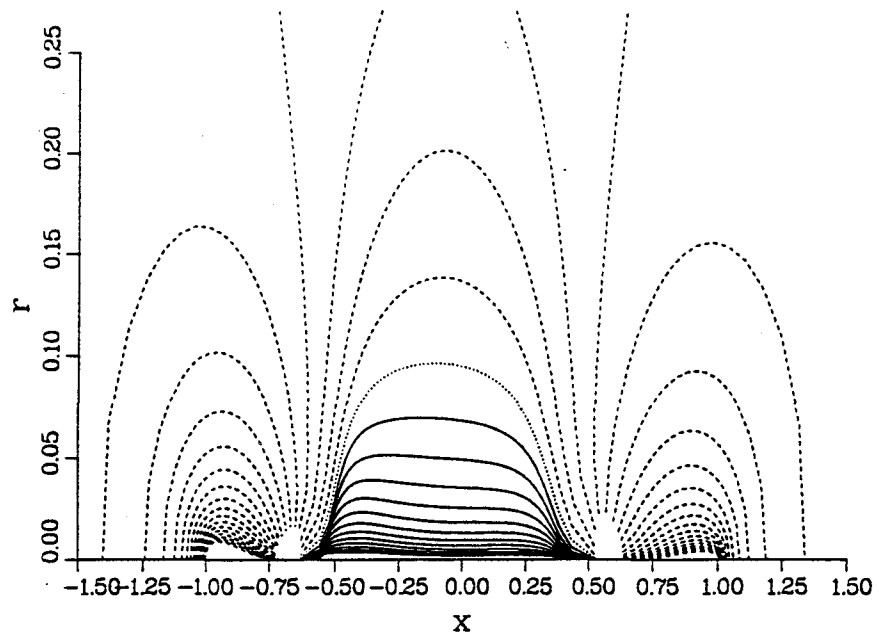
In Figure 4 the results for the computation of SFB-1, the first shock-free body of revolution computed by Buckmire^[4] are outputted. The sequence of sonic line data which led to the computation of SFB-1 is displayed in Figure 3. The equation of the designed sonic line is given by

$$R(0, \nu) = 0.023 \exp \left[\frac{-z^2}{1 - z^2} \right],$$

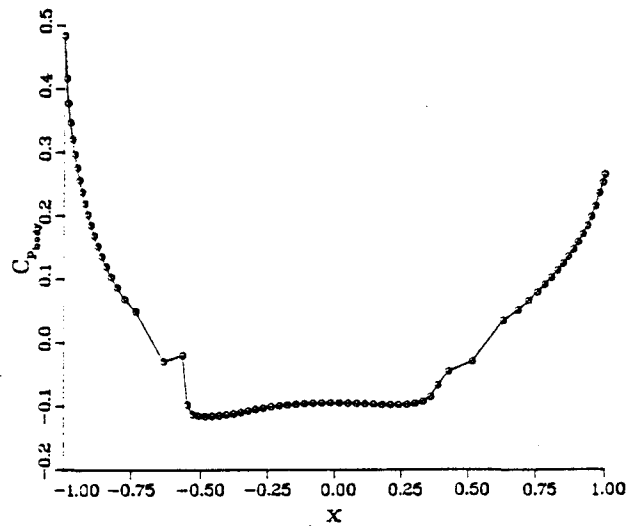
$$\text{where } z(\nu) = \frac{2\nu - 0.3052}{3.7648}.$$

The assumed body shape of $F(x) = (1 - x^2)(1 + \alpha x)$ with $\alpha = -0.1456$, results in $x_* = -0.63224$ and $x^* = 0.84792$, which corresponds to $\nu^* = -1.7298$ and $\nu_* = 2.0350$.

Let $\delta = 0.1$ and $M_\infty = 0.98025$ which corresponds to $K = 4.07$ and $\mathcal{D} = 3.4376$. In Figure 4 the approximate isobars and $C_{p_{body}}(x)$ are plotted. It is clear that no distinct shock is present. In other words, using design parameters and the algorithm enumerated in this paper, a shock-free flow has been numerically computed around SFB-1. However, the coarse nature of the numerical grid, especially near the points x^* and x_* where there is a rapid change of pressure occurring leads to questions of whether a very weak shock is forming at these extrema which is not being captured numerically. Cole & Malmuth^[7] have previously shown that if a shock is to develop on a transonic body of revolution, its location will be at one of the extrema of the source distribution function, x^* or x_* . The question of how the flow changes at off-design conditions is not fully resolved. In Buckmire^[4] there are numerical results to suggest that the flow remains essentially shock-free at non-design conditions. In a forthcoming paper the question of how the flow changes around a shock-free body at non-design speeds will be addressed.



(a) Isobars around SFB-1



(b) Pressure Coefficient on SFB-1

Figure 4: Data for shock-free body number 1, SFB-1

References

- [1] F. Bauer, P. Garabedian and D. Korn, *Supercritical Wing Sections*, Lecture Notes in Economics and Mathematical Systems, No. 66, Springer-Verlag, New York, 1972.
- [2] F. Bauer, P. Garabedian and D. Korn, *Supercritical Wing Sections II*, Lecture Notes in Economics and Mathematical Systems, No. 108, Springer-Verlag, New York, 1975.
- [3] F. Bauer, P. Garabedian and D. Korn, *Supercritical Wing Sections III*, Lecture Notes in Economics and Mathematical Systems, No. 150, Springer-Verlag, New York, 1977.
- [4] R. Buckmire, *The Design of Shock-free Transonic Slender Bodies of Revolution*, Ph.D. thesis, Rensselaer Polytechnic Institute, Troy, NY (1994).
- [5] R. Buckmire, *A new finite-difference scheme for singular differential equations in cylindrical or spherical coordinates*, Mathematics is for solving problems, Editors L. Pamela Cook, Victor Roytburd and Marshall Tulin, S.I.A.M. (1996) pp. 3-9.
- [6] J.D. Cole and L.P. Cook, *Transonic Aerodynamics*, North Holland, (1986).
- [7] J.D. Cole and N. Malmuth, *Shock Wave Location on a Slender Transonic Body of Revolution*, Mechanics Research Communications, 16(6), (1989), pp. 353-357.
- [8] J.D. Cole and A.F. Messiter, *Expansion Procedures and Similarity Laws for Transonic Flow*, Z.A.M.P., 8, (1957), pp. 1-25.
- [9] J.D. Cole and E.M. Murman, *Calculation of Plane Steady Transonic Flows*, AIAA Journal, Volume 9 Number 1, (January 1971), pp. 114-121.
- [10] J.D. Cole and D.W. Schwendeman, *Hodograph Design of Shock-free Transonic Slender Bodies*, 3rd International Conference on Hyperbolic Problems, Editors Bjorn Engqvist and Bertil Gustafsson, Uppsala, Sweden, (June 11-15 1990).
- [11] J.J. Kacprzynski, L. H. Ohman, P.R. Garabedian, and D.G. Korn, *Analysis of the Flow Past a Shockless Lifting Airfoil in Design and Off-design Conditions*, N.R.C. of Canada Aeronautical Report LR-554, Ottawa (1971).
- [12] J.J. Kacprzynski, *Wind Tunnel Test of the Shockless Lifting Airfoil No. 1*, Project Report 5x5/0062, National Research Council of Canada, Ottawa (1972).
- [13] J.J. Kacprzynski, *Wind Tunnel Test of the Shockless Lifting Airfoil No. 2*, Laboratory Technical Report LTR-HA-5x5/0067, National Research Council of Canada, Ottawa (1973).
- [14] J.A. Krupp and E.M. Murman, *Computation of Transonic Flows past Lifting Airfoils and Slender Bodies*, AIAA Journal, Volume 10 Number 7, (July 1972), pp. 880-886.
- [15] G.Y. Nieuwland, *Transonic potential flow around a family of quasi-elliptical sections*, Technical Report T. 172 (1967).
- [16] H.H. Pearcey, *The aerodynamic design of section shapes for swept wings*, Advances in Aeronautical Sciences, Vol. 3 (1962), London.
- [17] D.W. Schwendeman, *Hodograph Design in Transonic Flow*, Mathematics is for solving problems, Editors L. Pamela Cook, Victor Roytburd and Marshall Tulin, S.I.A.M., (1996) pp. 204-219.
- [18] H. Sobieczky, K.-Y. Fung, A.R. Seebass and N.J. Yu, *A New Method for Designing Shock-free Transonic Configurations*, AIAA J., 17, (1979) pp. 722-729.
- [19] R.T. Whitcomb and L. Clark, *An airfoil shape for efficient flight at supercritical Mach numbers*, NASA Tech. Man. X-1109 (1965).